Spin-domain formation in spinor Bose-Einstein condensation

Tomoya Isoshima,[1,*] Kazushige Machida,[1] and Tetsuo Ohmi[2]
[1]*Department of Physics, Okayama University, Okayama 700-8530, Japan*
[2]*Department of Physics, Graduate School of Science, Kyoto University, Kyoto 606-8502, Japan*
(Received 13 May 1999)

The spatial structure of the spinor Bose-Einstein condensates with the spin degrees of freedom is analyzed based on the generalized Gross-Pitaevskii (GP) equation in light of the present spin-domain experiment on $m_F=\pm 1$, and 0 of the hyperfine state $F=1$ of ^{23}Na atom gases. The GP solutions in three- and one-spatial dimensional cases reproduce the observed spin-domain structures, revealing the length scale associated with the existence of the weak interaction of the spin-spin channel, other than the ordinary coherence length related to the density-density channel. The obtained domain structure in GP is compared with the result in the Thomas-Fermi approximation. The former solution is found to better describe the observed features than the latter. [S1050-2947(99)02412-9]

PACS number(s): 03.75.Fi, 05.30.Jp

I. INTRODUCTION

The experiments for Bose-Einstein condensation (BEC) in alkali atomic gases, such as ^{87}Rb [1], ^{23}Na [2], and ^{7}Li [3], have been performed under a strong magnetic field since its experimental realization in alkali atomic gases in 1995. The the magnetic field was used to confine a BEC system. Because the atom spin direction adiabatically follows the magnetic field, the spin degrees of freedom are frozen in these magnetic trapping experiments [4].

Recently, the MIT group succeeded in creating BEC using an optical dipole trap formed by a single infrared laser beam [5–7] in which the spin degrees of freedom are all active ($m_F=1,0,-1$ of the $F=1$ atomic hyperfine state for ^{23}Na). These atoms with the three hyperfine substates simultaneously undergo Bose condensation, leading to a spinor BEC, a situation analogous to superfluid ^{3}He [8] of a neutral Fermion system or a triplet superconductor of a charged Fermion system such as UPt_3 [9]. The spin degrees of freedom play a fundamentally important role for governing their physics. An advantage of the present spinor BEC over ^{3}He or UPt_3 is that it is a weakly interacting system and we know fairly well how the (quasi)particles interact using the knowledge of atomic physics. These facts allow us the chance to construct a microscopic many-body theory from first principles, using only a few fundamental matter parameters.

Stimulated by the earliest optical trap experiment by Stumper-Kurn *et al.* [5], general theoretical frameworks for describing a spinor BEC were given independently by Ohmi and Machida [10] and by Ho [11]. They are equivalent basically. The framework is based on Bogoliubov theory which is extended to a vectorial order parameter with three components, corresponding to $m_F=1,0,-1$ of the $F=1$ atomic hyperfine state, giving rise to generalized Gross-Pitaevskii (GP) equation. They calculate low-lying collective modes such as sound wave, spin wave, and their coupled mode and predict various topological defect structures, or spin textures. We also note that there is much remarkable research [12] into the phase separation problem of a two-component BEC consisting of different hyperfine states.

Subsequently, Stenger *et al.* [6] produced an optically trapped spinor BEC with a long cigar shape whose aspect ratio is over 40 and examine whether these three-component BEC's can be either miscible or immiscible. The external magnetic field is applied along the long axis (the z axis) to see the spin-domain formation. After releasing the spinor BEC, the Stern-Gerlach separation of the cloud is performed to reproduce the original domain structure. Their analyses are based on the Thomas-Fermi (TF) approximation, which neglects the kinetic energy of the above generalized GP equations. They conclude that the spin-dependent interaction channel of the present spinor BEC is antiferromagnetic, rather than ferromagnetic in this particular hyperfine state.

In this paper, we analyze the above experiment by Stenger *et al.* [6] in more detail to determine the three-dimensional structure of the domain wall including the miscible and immiscible spin-domain structures. The one-dimensional calculation is also done in order to discuss the characteristic lengths. The arrangement of the paper is as follows. In Sec. II, we introduce the generalized Gross-Pitaevskii equation of a Bose-Einstein condensed system with internal spin degrees of freedom. In Sec. III we simulate the actual experimental system in light of the experimental conditions of Ref. [6] and investigate three-dimensional systems. The properties of a one-dimensional system in an idealized situation are explored in Sec. IV. The last section is devoted to a summary and conclusion.

II. FORMULATION

The Hamiltonian invariant under spin space rotation and gauge transformation is written in terms of the three-component field operators: $\Psi_{+1},\Psi_0,\Psi_{-1}$, corresponding to the sublevels $m_F=+1,0,-1$ of the hyperfine state $F=1$. Namely, it is given by

*Electronic address: tomoya@mp.okayama-u.ac.jp

$$\mathrm{H}=\int d\mathbf{r}\sum_i \Psi_i^\dagger(\mathbf{r})h_i(\mathbf{r})\Psi_i(\mathbf{r}) + \frac{g_n}{2}\sum_{i,j}\Psi_i^\dagger(\mathbf{r})\Psi_j^\dagger(\mathbf{r})\Psi_j(\mathbf{r})\Psi_i(\mathbf{r}) + \frac{g_s}{2}\sum_\alpha\left(\sum_{i,j}\Psi_i^\dagger(\mathbf{r})(F_\alpha)_{i,j}\Psi_j(\mathbf{r})\right)^2, \tag{1}$$

where

$$h_i(\mathbf{r})=-\frac{\hbar^2\nabla^2}{2m}-\mu+V(\mathbf{r})-p(F_z)_{i,i}+q(F_z^2)_{i,i} \tag{2}$$

is the one-body Hamiltonian, $V(\mathbf{r})$ is the trapping potential, $i,j=0,\pm1$ are spin indices and $F_\alpha(\alpha=x,y,z)$ are the following 3×3 spin matrices:

$$F_x=\frac{1}{\sqrt{2}}\begin{pmatrix}0&1&0\\1&0&1\\0&1&0\end{pmatrix}, \tag{3}$$

$$F_y=\frac{i}{\sqrt{2}}\begin{pmatrix}0&-1&0\\1&0&-1\\0&1&0\end{pmatrix}, \tag{4}$$

$$F_z=\begin{pmatrix}1&0&0\\0&0&0\\0&0&-1\end{pmatrix}. \tag{5}$$

We have introduced the linear and quadratic Zeeman energies [6], $E_{\mathrm{ze}}=E_0-\tilde{p}\langle F_z\rangle+q\langle F_z^2\rangle$ with $p\equiv\tilde{p}+p_0$ and the Lagrange multiplier p_0 represents the conservation of the total spin of the system.

The interaction constants are related to the two kinds of scattering lengths a_0 and a_2 corresponding to the total spin zero channel and two channel:

$$g_n=\frac{4\pi\hbar^2}{m}\frac{a_0+2a_2}{3}, \tag{6}$$

$$g_s=\frac{4\pi\hbar^2}{m}\frac{a_2-a_0}{3}. \tag{7}$$

Let us introduce the three-component order parameters: $\phi_i=\langle\Psi_i\rangle$ with $i=x,y,z$. Following the standard procedure [13], we can derive the Gross-Pitaevskii equation for describing $\phi_i(\mathbf{r})$ from the Hamiltonian Eq. (1):

$$\left[h_i(\mathbf{r})+g_n\sum_j|\phi_j(\mathbf{r})|^2\right]\phi_i(\mathbf{r}) + g_s\sum_\alpha\sum_{j,k,l}(F_\alpha)_{i,j}\phi_j\phi_k^*(F_\alpha)_{k,l}\phi_l=0. \tag{8}$$

The energy of the system is given by

$$E=\int d\mathbf{r}\sum_i\{\phi_i^*(\mathbf{r})h_i(\mathbf{r})\phi_i(\mathbf{r})\}+\int d\mathbf{r}\{E_n(\mathbf{r})+E_s(\mathbf{r})\}, \tag{9}$$

where

$$E_n(\mathbf{r})=\frac{g_n}{2}\sum_i|\phi_i(\mathbf{r})|^4, \tag{10}$$

$$E_s(\mathbf{r})=\frac{g_s}{2}\sum_\alpha\left(\sum_{i,j}\phi_i^*(\mathbf{r})(F_\alpha)_{i,j}\phi_j(\mathbf{r})\right)^2. \tag{11}$$

We will use the following notation in Sec. IV: $\zeta_i(\mathbf{r})=\phi_i(\mathbf{r})/\sqrt{n(\mathbf{r})}$ where $n(\mathbf{r})=\Sigma_i|\phi_i|^2$.

It is possible to think that some spin-dependent type of inelastic collisions affect the behavior of this spinor BEC. But in this paper, we concentrate on how the GP equations describe the spinor system.

III. THREE-DIMENSIONAL CASE

In this section we analyze the three-dimensional systems in comparison with the actual experiments done by Stenger *et al.* [6]. The main interests are (1) the z position of the domain wall, and (2) the radial shape including the mutual overlapping of the spin domains.

A. Experiment

In order to establish a model system we briefly explain their experimental conditions. The condensate is under the magnetic field $B(z)$ which is applied along the z axis. Since the atoms are in the hyperfine $F=1$ state, the condensate consists of the three components: ϕ_{+1}, ϕ_0, and ϕ_{-1}. The nonuniform magnetic field $B(z)$ is characterized by its field gradient: $p'\propto dB(z)/dz$. The p in E_{ze} is set to zero at $z=0$ and $p=p'z$. The stronger-field side of the cigar-shaped condensate is filled with the $+1$ condensate. As the system follows the total spin conservation, the opposite side is filled with the -1 condensate. Stenger *et al.* [6] observe the column density distribution of the three spin components and estimate the interaction constant g_s from the z position of the domain wall between the spin components. The result depends not only on p, but also on the coefficient q. $q\propto B_0^2$ where $B_0\simeq B(z)$ is the base magnetic field. The experiments are done for various p's and q's. From Fig. 4 of Ref. [6], $p'=1$ Hz/μm and $q=2$ Hz corresponds to $dB/dz\sim1.4\times10^{-3}$ mG/μm and $B_0\sim20$ mG. Because the system size <300 μm, we can treat p' and q as constant even in this weak B_0.

They estimate the relationship of p and q to the z position of the domain wall by approximating the cigar-shaped system as a one-dimensional one with uniform density, which is assumed to be 2/3 times the peak density. The kinetic term is also ignored. This allows us to draw lines in p-q phase diagram as a function of the interaction constant g_s (in their paper, c_2).

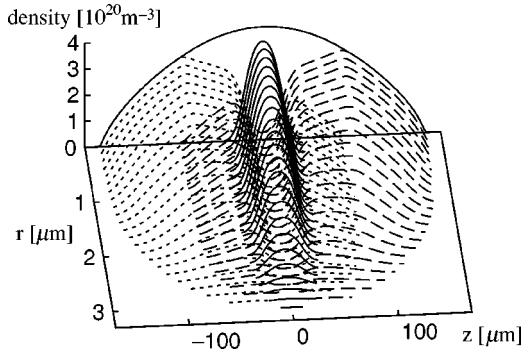

FIG. 1. The density plot of the r-z plane. The dashed lines, the solid lines around $z=0$, and the dotted lines indicate the densities of the $+1$, 0, and -1 components. The upper solid curve at $r=0$ indicates the total density at $r=0$. The peak density is 4.35×10^{20} m^{-3}, $p'=1.0$ Hz/μm, and $q=2.0$ Hz. The optical confinement is assumed as the harmonic potential given by $V(\mathbf{r})=m/2\{(2\pi\nu_r r)^2+(2\pi\nu_z z)^2\}$, where $\nu_z=15$ Hz and $\nu_r=900$ Hz. The total particle number is 8.71×10^5.

B. Calculation

In order to check whether or not their analysis based on the above assumptions (one-dimensional TF approximation, 1DTF) agrees with the full three-dimensional calculations of the GP equation, we determine the spatial profiles of the rotationally symmetric (around the z axis) spinor condensate by solving the GP equation in the r-z space using the difference between the scattering lengths $a_2-a_0=0.19$ nm ($\propto g_s$) and the peak density $n_{\rm peak}=4.35\times10^{20}m^{-3}$ they estimated. We treated the magnetic-field parameters p' and q as constants of each system calculated and they do not vary spatially. Assuming these, we compare the calculations by 1DTF, by three-dimensional TF approximation (3DTF), and by three-dimensional GP equation (3DGP). In 1DTF, it is assumed that the density is $\frac{2}{3}n_{\rm peak}$.

We first discuss the domain structure along the r direction and the mutual overlapping between the three components. One example ($p'=1.0$ Hz/μm, $q=2.0$ Hz) of the calculated results with 3DGP is depicted in Figs. 1 and 2(a). There is a large overlapping region consisting of the $+1$ and the -1 components, between the region consisting of the $+1$ (or -1) component only and of the 0 component only. In other words, the double-peak structures of the -1 component and $+1$ component are situated at both the $z>0$ side and $z<0$ side in Figs. 1 and 2(a). This feature is in accord with the observation (Fig. 3 in [6]). Figure 2(a) also shows that the condensate itself allows the overlapping of three components at $z=0$ in certain values of p' and q. This existence of three components at $z=0$ does not occur in calculations with 3DTF [e.g., Fig. 2(b)]. Usually the difference between the results of the TF approximation and of the full GP equation is considered to be an order of the coherence length ~1 μm here, but the difference between the two treatments is as long as 50 μm, which is far longer than expected. This behavior also occurs in the one-dimensional system and is discussed thoroughly at Sec. IV. (This overlapping at $r=0$ does not occur at larger q, but the length scale stays as long as 10 μm.)

Another interesting difference between the results from 3DTF and 3DGP exists at the crossing point between the 0 component and the $+1$ component. As seen in Fig. 2(a), the z coordinates of the crossing points do not move appreciably between the two cases: $r=0$ and $r=2$. However, the crossing point moves significantly in TF as seen from Fig. 2(b). The trace of these crossing points in the r-z plane for various radial harmonic potentials are depicted in Fig. 3.

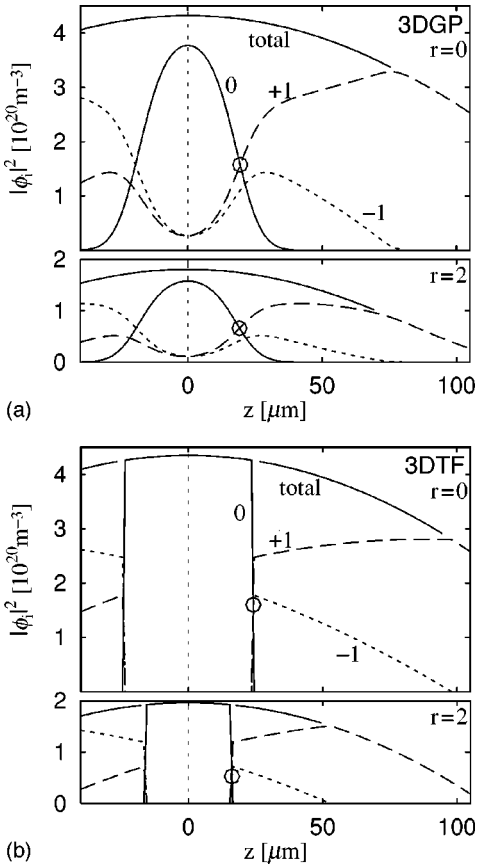

FIG. 2. The density profiles of the condensate. The peak density, p, q, and the shape of the harmonic confinement are the same as in Fig. 1 except for the total particle number 8.99×10^5 in (b). The dashed lines, the solid lines around $z=0$, and the dotted lines indicate the densities of the $+1$, 0, and -1 components. The upper solid curves indicate the total density. (a) The density profile at $r=0$ and 2 μm. The ±1 components exist even at $z=0$. We call the crossing between the 0 and $+1$ components (circles) the domain wall. The z coordinates of the domain wall are $z=19.5$ μm at $r=0$ and $z=19.2$ μm at $r=2$ μm. (b) The density profile when calculated with 3DTF. As r increases, the domain wall (circles) between the 0 component and ±1 components moves toward $z=0$. The z coordinates of the domain wall are $z=24.1$ μm at $r=0$ and $z=16.2$ μm at $r=2$ μm.

C. Phase diagram

To compare the z position of the domain wall between the 0 component and the 1 component, we integrate the density profile, e.g., Fig. 1 along the r surface. Figure 4(a) shows an example of the results in 3DGP and Fig. 4(b) shows that in 3DTF. When the density profile is integrated along the r direction this produces further overlapping between the components especially in 3DTF [compare Fig. 2(b) with Fig. 4(b)]. As seen from Fig. 4(a), the z coordinate of the crossing point in 3DGP is slightly smaller than the 3DTF case in Fig. 4(b).

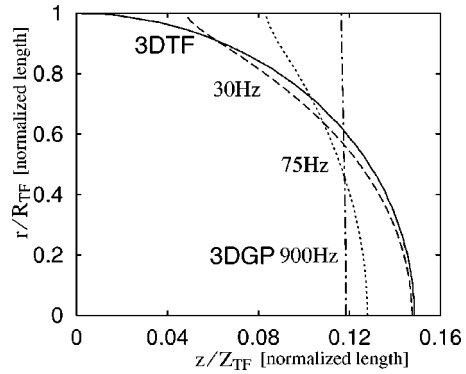

FIG. 3. The crossing point of the 0 component and the $+1$ component for $\nu_r=30$, 75, and 900 Hz. The solid line, which is independent of ν_r, is the line when the TF approximation is used. The 900 Hz line corresponds to Fig. 1. Each axis is normalized by the TF radius and length, which are defined as (peak density)$\times g_n = m/2(2\pi\nu_r R_{\rm TF})^2 = m/2(2\pi\nu_z Z_{\rm TF})^2$. The $R_{\rm TF}$ is 82.2, 32.9, and 2.74 μm for $\nu_r=30$, 75, and 900 Hz, respectively. $Z_{\rm TF}$ is 164 μm.

The acquired z values of 3DTF for various p' and q values are shown in Fig. 5(a). The 1DTF line $p=2\sqrt{50.7q}$ is also plotted. The value 50.7 is derived uniquely from the assumed scattering lengths and the peak density ($\times 2/3$). No significant difference is seen. The lower branch lines in Fig. 5 comes from the density profile along the z axis; When z is large, the value 50.7 ($\propto$ density) must become much smaller. Figure 5(b) compares the 1DTF and the 3DTF.

The differences in p-q diagram between 1DTF, 3DTF, and 3DGP are small. Therefore, we conclude that the estimate in Ref. [6] is correct. But the shapes of domain walls are not simple as shown in Figs. 2 and 3.

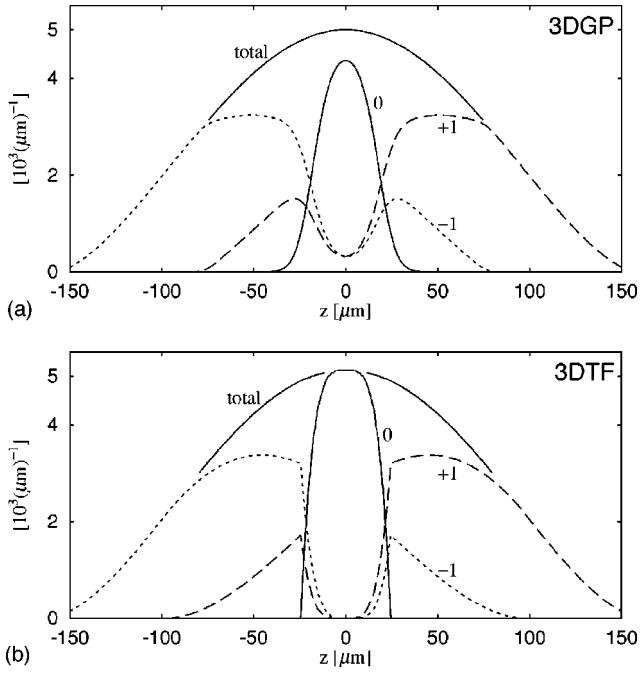

FIG. 4. (a) The r-integrated density profiles for $p'=1.0$ Hz/μm and $q=2.0$ Hz. The overlapping of these integrated densities simply reflects the shape of Fig. 2(a). The z coordinate of the domain wall is 19.3 μm. (b) The corresponding result for 3DTF. The overlapping of these integrated densities comes from the r-dependent shift of the domain wall depicted in Fig. 3. The z coordinate of the domain wall is 21.5 μm. These figures should be compared with Fig. 3 in [6].

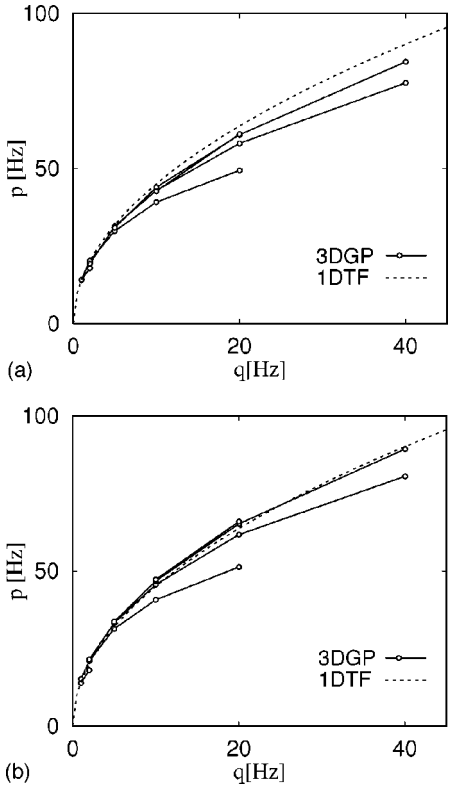

FIG. 5. The p-q diagram. (a) Comparison between the the results in 1DTF and 3DGP. (b) Comparison between the results in 1DTF and 3DTF. The magnetic-field parameters are $p'=0.2$, 0.5, 1, 2, and 4 Hz/μm, and $q=1$, 2, 5, 10, 20, and 40 Hz (not all of the combinations are used). The 1DTF line is $p=2\sqrt{50.7q}$.

IV. ONE-DIMENSIONAL CASE

We have seen in the preceding section that the difference between the density distributions by the TF result and GP result is much wider than the usual coherence length $\xi \lesssim 1$ μm. In this section, we take up the one-dimensional system to investigate why this is so, taking into account the effects of the kinetic term and the interaction g_s term. The magnetic-field coefficients (p and q) and the optical potential $V(\mathbf{r})$ are set to zero in this section. The kinetic term, the interaction (g_n and g_s) terms, and the chemical potential μ are retained.

A. Positive g_s

Figures 6(a) and 6(b) show the cases in which g_s is positive. The ratio of the components is fixed at each end of the system; $(\zeta_{+1},\zeta_0,\zeta_{-1})=(0,1,0)$ at the left-hand edge and $(1,0,0)$ at the right-hand edge of the system. We impose an additional condition that the ζ_{-1} component is zero in Fig. 6(a). In this case, the overlapping between ζ_0 and ζ_{+1} is seen to be an order of a few micrometers. This length scale can be explained by $\xi_s \equiv \sqrt{3/8\pi n(a_2-a_0)}$, which is about 1.2 μm in the present case. Figure 6(b) shows that when no compo-

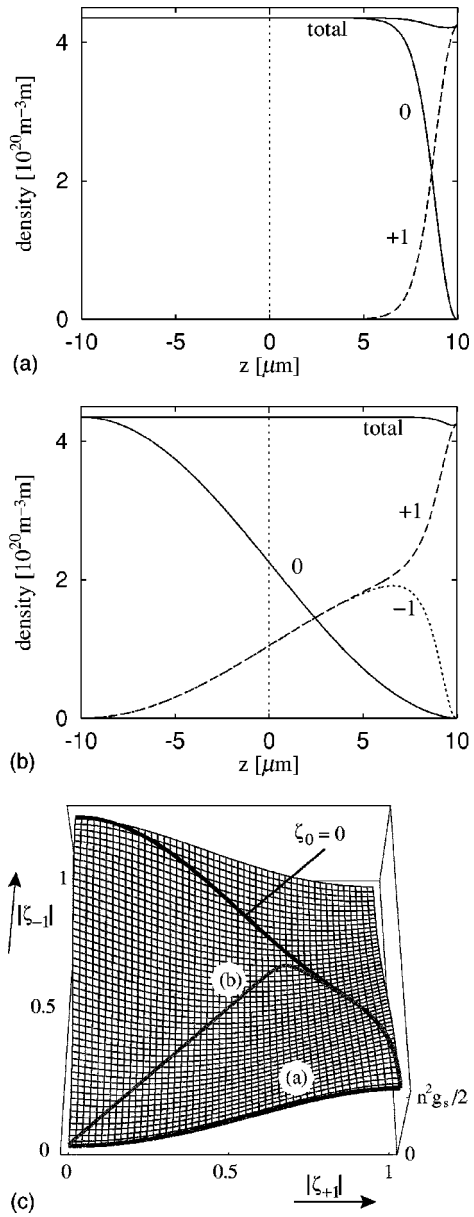

FIG. 6. The one-dimensional systems with positive $g_s(a_0 = 2.75$ nm, $a_2 = 2.94$ nm). The chemical potential μ is 4.35×10^{20} m$^{-3}\times g_n$. (a) The density variation of the three components when the boundary condition $(|\zeta_{+1}|,|\zeta_0|,|\zeta_{-1}|)=(1,0,0)$ at $z=-10$ μm and $(0,1,0)$ at $z=10$ μm is imposed. We suppress ζ_{-1} over whole range of z. (b) The density variation of the three components when the boundary condition is imposed that $(|\zeta_{+1}|,|\zeta_0|,|\zeta_{-1}|)=(1,0,0)$ at $z=-10$ μm and $(0,1,0)$ at $z=10$ μm. (c) The landscape of E_s. The labels (a) and (b) correspond to the above figures, (a) and (b), respectively.

nent is suppressed, the overlapping region becomes wider and is subdivided into the wider region (-10 μm$<z<5$ μm) where $\zeta_{-1}=\zeta_{+1}$ and the narrow region (5 μm$<z<10$ μm) where $\zeta_{-1}\neq\zeta_{+1}$. The latter region is characterized by the coherence length ξ_s.

The difference between Figs. 6(a) and 6(b) is explained by considering the E_s term of the total energy [Eq. (9)]. The relative phases of ζ's (equivalently, of ϕ's) are determined under the condition that E_s is minimized as shown in the Appendix. We can write E_s as

$$E_s=\frac{n^2(\mathbf{r})g_s}{2}\sum_{\alpha}\left(\sum_{i,j}\zeta_i^*(\mathbf{r})(F_\alpha)_{i,j}\zeta_j(\mathbf{r})\right)^2$$
$$=\frac{n^2g_s}{2}[-(|\zeta_{+1}|\pm|\zeta_{-1}|)^4+2(|\zeta_{+1}|\pm|\zeta_{-1}|)^2]. \quad (12)$$

The upper and lower signs correspond to the positive and negative g_s, respectively. Equation (12) shows that E_s is minimum on the line $|\zeta_{+1}|=|\zeta_{-1}|$ when $g_s>0$, and on $|\zeta_{+1}|+|\zeta_{-1}|=1$ when $g_s<0$.

Figure 6(c) shows the landscape of E_s when $g_s>0$. The gray lines (a) and (b) in Fig. 6(c) correspond to Figs. 6(a) and 6(b), respectively. The line (b) goes along the minimum energy line $|\zeta_{+1}|=|\zeta_{-1}|$ at first and this corresponds to the $z=-10$ μm to 5 μm region in Fig. 6(b). Both the lines (a) and (b) climb up the hill in the E_s landscape from $E_s=0$ to $E_s=n^2g_s/2$. This process is controlled by the kinetic term and the interaction g_s term in the GP equation, Eq. (8), and the length scale is an order of ξ_s.

The spatial variation in Fig. 6(b) is also understood by the so-called d vector [8], which expresses the spin structure of superfluid. At $z=-10$ μm and $z=10$ μm the d vectors are given by $d=\hat{z}$ and $d=\hat{x}+i\hat{y}$, respectively. In the region from $z=-10$ μm to 5 μm the d vector rotates from the z direction to the x direction. Since these states are energetically degenerate, this length scale is governed by the system size. On the other hand, in the region from $z=5$ μm to $z=10$ μm the d vector is described by $d=\hat{x}+it\hat{y}$ where t varies from $t=0$ ($z=5\mu$m) to $t=1$ ($z=10$ μm). This state change produces the energy variation related to the interaction g_s, thus is governed by the spin-coherence length ξ_s.

B. Negative g_s

Figure 7 shows the cases in which g_s is negative. In Fig. 7(a), the ratio of the components is fixed to $(|\zeta_{+1}|,|\zeta_0|,|\zeta_{-1}|)=(0,0,1)$ at the left-hand edge and $(1,0,0)$ at the right-hand edge of the system. As shown by the gray line (a) in Fig. 7(c), the system goes along the minimum E_s line $|\zeta_{+1}|+|\zeta_{-1}|=1$. Therefore, the length scale is not controlled by ξ_s and it becomes as long as the boundary conditions allow, that is, the length scale is determined by the boundary condition. This gentle shape contrasts remarkably with Fig. 7(b) which shows the system when the ratio of the components is fixed to $(|\zeta_{+1}|,|\zeta_0|,|\zeta_{-1}|)=(0,0,1)$ at the left-hand edge of the system. The quick change around $z=-10$ μm to -7 μm is controlled by ξ_s in a similar reason of the previous $g_s>0$ case. It is interesting to note that the ζ_{-1} component spontaneously appears to minimize E_s; the system without restriction does not go along the $|\zeta_{-1}|=0$ line.

C. Length scales

The length scale of the density variation in the system *without* the spin freedom is determined by $\xi=\sqrt{1/(8\pi na)}$ where $a(>0)$ is the s-wave scattering length. This is equivalent to $\xi_n\equiv\sqrt{3/8\pi n(2a_2+a_0)}$ (where $2a_2+a_0>0$) in the system treated in this paper. The origin of ξ_n is the competition between the kinetic term and the interaction term with g_n in the GP equation.

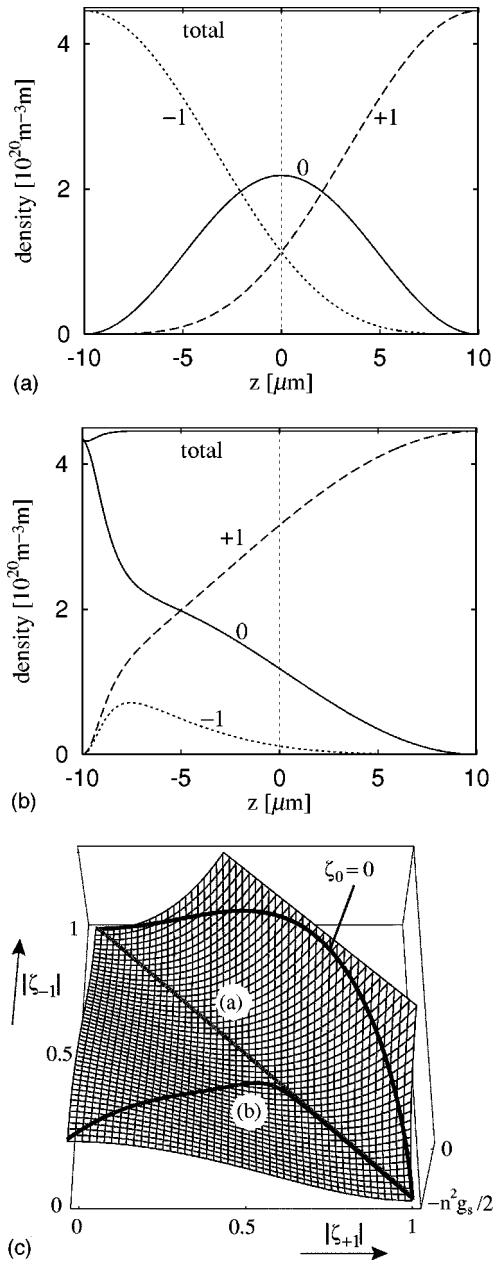

FIG. 7. The one-dimensional systems with negative g_s ($a_0 = 2.75$ nm, $a_2 = 2.56$ nm). The chemical potential μ is 4.35×10^{20} m$^{-3}\times g_n$. (a) The density variation of the three components when the boundary condition is imposed that $(|\zeta_{+1}|,|\zeta_0|,|\zeta_{-1}|)=(0,0,1)$ at $z=-10$ μm and $(1,0,0)$ at $z=10$ μm. (b) The density variation of the three components when the boundary condition is imposed that $(|\zeta_{+1}|,|\zeta_0|,|\zeta_{-1}|)=(0,1,0)$ at $z=-10$ μm and $(1,0,0)$ at $z=10$ μm. (c) The landscape of E_s. The labels (a) and (b) correspond to the above figures, (a) and (b), respectively.

On the other hand, there are three types of length scales in system with the spin freedom.

(1) ξ_n, which is explained above. This becomes dominant when the total density varies. This is not significant in these one-dimensional systems because their densities are almost uniform. In three-dimensional calculations, the *total* density profile along the *r* axis in Fig. 1, which is gentler than that in 3DTF (no corresponding figure in this paper), is explained by ξ_n.

(2) ξ_s. When the total density does not vary significantly, this length scale becomes important. The origin is the competition between the g_s term, Figs. 6(c) and 7(c) for example, and the kinetic term in the GP equation. This length is seen in Fig. 6(a) and the left-hand side of Fig. 7(b).

(3) There is another length controlled by the kinetic term, and conditions other than g_n and g_s. In this model system, ''conditions'' means the boundary conditions at each edge. When the spin state of the system varies along the lowest energy line of E_s and the total density does not vary, the length scale of the density variation of the components is governed by neither g_n nor g_s. In other words, by neither (1) ξ_n nor (2) ξ_s. The characteristic length is controlled by the boundary conditions in the one-dimensional cases: the left-hand side of Fig. 6(b) and Fig. 7(a). They correspond to the line (b) in Fig. 6(c) and the line (a) in Fig. 7(c).

As for the previous three-dimensional calculations, type (3) of these length scales explains the difference between the results of the 3DGP and the 3DTF in Figs. 2(a) and 2(b). The magnetic-field parameters *p* and *q* determine the characteristic length when 3DGP is used. It is neither ξ_n nor ξ_s. We note that the ζ_{+1} and ζ_{-1} components have the finite density at $z=0$ in Fig. 2(a). This long length scale is explained by the minimum energy line of the g_s term in the GP equation (or E_s). This is the $|\zeta_{-1}|=|\zeta_{+1}|$ line of Fig. 6(c).

V. SUMMARY AND CONCLUSION

We have investigated the spinor BEC systems based on the generalized GP equation extended to the cases where the BEC has the spin degrees of freedom. The spatial structure of the domain wall which is the interface of the different spin states of BEC is analyzed by solving the GP equation for both rotationally symmetric (around the *z* axis) three-dimensional and one-dimensional cases. The former case simulates the actual experimental situation of Stenger *et al.* [6]. Our calculations show that the simple TF approximation taken by Stenger *et al.* can be justified and yields the correct value of the interaction constant of the spin channel which turns out to be antiferromagnetic in the present hyperfine state $F=1$ of ^{23}Na atoms. The full GP solutions in both three- and one-dimensional cases reveal a long length scale associated with the interaction of the spin channel, yielding the large overlapping region between the immiscible components (e.g., 0 and $+1$).

ACKNOWLEDGMENT

The authors thank S. Inouye for valuable discussions on their spin-domain experiments.

APPENDIX: RELATIVE PHASES OF ϕ

The relative phases of the three component condensate wave functions are determined such that the energy density of the g_s term

$$E_s=\frac{g_s}{2}\sum_{\alpha}\left(\sum_{i,j}\phi_i^*(F_\alpha)_{i,j}\phi_j\right)^2 \qquad \text{(A1)}$$

is minimized under the condition that the amplitudes of ϕ are fixed. This is because the other terms in E are not affected by the choice of phases. We assume that

$$(\phi_1,\phi_0,\phi_{-1})=(\beta_1 e^{i\gamma_1},\beta_0,\beta_{-1}e^{i\gamma_{-1}}), \tag{A2}$$

where $\beta_i(\geqslant 0)$ and γ_i are real numbers. The amplitudes β_i are fixed and we determine γ_i to minimize E_s. From Eq. (A1) we obtain

$$\begin{aligned}\frac{2E_s}{g_s}&=\frac{\phi_0^2}{2}[(\phi_1^*+\phi_1+\phi_{-1}+\phi_{-1}^*)^2-(\phi_1^*-\phi_1+\phi_{-1}-\phi_{-1}^*)^2]+(|\phi_1|^2-|\phi_{-1}^2|^2)^2\\&=\frac{\beta_0^2}{2}[(2\beta_1\cos\gamma_1+2\beta_{-1}\cos\gamma_{-1})^2+(2\beta_1\sin\gamma_1-2\beta_{-1}\sin\gamma_{-1})^2]+(\beta_1^2-\beta_{-1}^2)^2\\&=2\beta_0^2[\beta_1^2+\beta_{-1}^2+2\beta_1\beta_{-1}\cos(\gamma_1+\gamma_{-1})]+(\beta_1^2-\beta_{-1}^2)^2.\end{aligned} \tag{A3}$$

When $g_s>0$, E_s is minimized with $\gamma_1+\gamma_{-1}=\pi$. Therefore, we can take ϕ as

$$(\phi_1,\phi_0,\phi_{-1})=(\beta_1,\beta_0,-\beta_{-1}). \tag{A4}$$

When $g_s<0$, $\gamma_1+\gamma_{-1}=0$. Therefore,

$$(\phi_1,\phi_0,\phi_{-1})=(\beta_1,\beta_0,\beta_{-1}). \tag{A5}$$

[1] M. H. Anderson, J. R. Ensher, M. R. Mathews, C. E. Wieman, and E. A. Cornell, Science **269**, 198 (1995).

[2] K. B. Davis, M.-O. Mewes, M. R. Andrews, N. J. van Druten, D. D. Durfee, D. M. Kurn, and W. Ketterle, Phys. Rev. Lett. **75**, 3969 (1995).

[3] C. C. Bradley, C. A. Sackett, J. J. Tollett, and R. G. Hulet, Phys. Rev. Lett. **75**, 1687 (1995); see, also, more recent experiment on this system: C. C. Bradley, C. A. Sackett, and R. G. Hulet, *ibid.* **78**, 985 (1997); **78**, 1170(E) (1997).

[4] See for review F. Dalfovo, S. Giorgini, L. P. Pitaevskii, and S. Stringari, Rev. Mod. Phys. **71**, 463 (1999).

[5] D. M. Stamper-Kurn, M. R. Andrews, A. P. Chikkatur, S. Inouye, H.-J. Miesner, J. Stenger, and W. Ketterle, Phys. Rev. Lett. **80**, 2027 (1998).

[6] J. Stenger, S. Inouye, D. M. Stamper-Kurn, H.-J. Miesner, A. P. Chikkatur, and W. Ketterle, Nature (London) **396**, 345 (1998).

[7] H.-J. Miesner, D. M. Stamper-Kurn, J. Stenger, S. Inouye, A. P. Chikkatur, and W. Ketterle, Phys. Rev. Lett. **82**, 2228 (1999).

[8] D. Vollhardt and P. Wölfle, *The Superfluid Phases of He 3* (Taylor-Francis, London, 1990).

[9] K. Machida and T. Ohmi, J. Phys. Soc. Jpn. **67**, 1122 (1998).

[10] T. Ohmi and K. Machida, J. Phys. Soc. Jpn. **67**, 1822 (1998).

[11] T.-L. Ho, Phys. Rev. Lett. **81**, 742 (1998).

[12] E. Timmermans, Phys. Rev. Lett. **81**, 5718 (1998); B. D. Esry, C. H. Greene, J. P. Burke, and J. L. Bohn, *ibid.* **78**, 3594 (1997); P. Ao and S. T. Chui, Phys. Rev. A **58**, 4836 (1998).

[13] See, for example, A. L. Fetter and J. D. Walecka, *Quantum Theory of Many-Particle Systems* (McGraw-Hill, New York, 1971).